Q. J. Ge
Computational Design Kinematics Laboratory,
Department of Mechanical Engineering,
Stony Brook University,
Stony Brook, NY 11794-2300

Anurag Purwar[1]
Computational Design Kinematics Laboratory,
Department of Mechanical Engineering,
Stony Brook University,
Stony Brook, NY 11794-2300
e-mail: anurag.purwar@stonybrook.edu

Ping Zhao
Computational Design Kinematics Laboratory,
Department of Mechanical Engineering,
Stony Brook University,
Stony Brook, NY 11794-2300

Shrinath Deshpande
Computational Design Kinematics Laboratory,
Department of Mechanical Engineering,
Stony Brook University,
Stony Brook, NY 11794-2300

A Task-Driven Approach to Unified Synthesis of Planar Four-Bar Linkages Using Algebraic Fitting of a Pencil of G-Manifolds

This paper studies the problem of planar four-bar motion generation from the viewpoint of extraction of geometric constraints from a given set of planar displacements. Using the image space of planar displacements, we obtain a class of quadrics, called generalized- or G-manifolds, with eight linear and homogeneous coefficients as a unified representation for constraint manifolds of all four types of planar dyads, RR, PR, and PR, and PP. Given a set of image points that represent planar displacements, the problem of synthesizing a planar four-bar linkage is reduced to finding a pencil of G-manifolds that best fit the image points in the least squares sense. This least squares problem is solved using singular value decomposition (SVD). The linear coefficients associated with the smallest singular values are used to define a pencil of quadrics. Additional constraints on the linear coefficients are then imposed to obtain a planar four-bar linkage that best guides the coupler through the given displacements. The result is an efficient and linear algorithm that naturally extracts the geometric constraints of a motion and leads directly to the type and dimensions of a mechanism for motion generation. [DOI: 10.1115/1.4035528]

1 Introduction

In this paper, we present a task-driven approach to unified type and dimensional synthesis of planar four-bar linkage mechanisms. Planar linkages are the most common form of mechanisms found in mechanical systems and have been a subject of interest and research in machine design area for many decades. Some key texts that describe state of the art as well as established methods and theory in kinematic synthesis of machines are by McCarthy and Soh [1], Sandor and Erdman [2], Hunt [3], Hartenberg and Denavit [4], and Suh and Radcliffe [5]. Despite having been a research topic alive for a long time, various proposed solutions to planar mechanism design for the approximate motion synthesis have been nonlinear in nature. In general, the algorithms proposed are computationally expensive and require dealing with the type and dimension synthesis separately. In this paper, we follow Wu et al. [6] and study the problem of planar motion approximation from the viewpoint of kinematic extraction of geometric constraints from a given set of planar displacements. Using a kinematic mapping of planar kinematics, we propose a general algebraic method for unified type and dimensional synthesis of planar four-bar linkages, which reveals the geometric constraints implicit in the given motion via a linear, two-step process. The method is fast, efficient, and provides type and dimensions of the mechanisms, which can execute that motion. This paper is an extension of our earlier work on dimensional synthesis of planar 4*R* linkages [7], wherein our focus was only on the motions that could be executed by *RR* dyads. The main contributions of this work are in (1) presenting a unified representation for the motion of all possible planar dyads, and (2) devising a simple linear method for naturally extracting the constraints hidden in a given motion and matching it with a four-bar motion without presumption of the type of a linkage. In addition, we also show via an example as to how the approach for four-bar linkage synthesis can be applied to six-bar linkages as well.

The earliest approach to the motion synthesis problem was dealt with by Burmester [8], who posited that a given four-bar linkage can go through at most five positions exactly (precision position synthesis). For a continuous motion or more than five positions, typically only an approximate motion synthesis can be performed. For this problem, Ravani and Roth [9,10] proposed a kinematic mapping approach. Blaschke [11] and Grunwald [12] had given rise to the concept of kinematic mapping almost a century ago, but it did not find many practical applications until the work of Ravani and Roth. A modern treatment of kinematic mapping can be found in the formative texts of Bottema and Roth [13] and McCarthy [14]. In the kinematic mapping approach to synthesis, planar displacements in Cartesian space are mapped into points in a three-dimensional projective space (called image space of planar kinematics), while workspace constraints of a mechanism map into algebraic manifolds (called constraint manifold) in the same space. In this way, a single degree-of-freedom (DOF) motion of a planar mechanism is represented by the intersection curve of two algebraic surfaces in the image space. The problem of motion approximation is transformed into an algebraic curve fitting problem in the image space, where various methods in approximation theory may be applied. This includes the definition of the approximation error (called structural error) in the image space, formulation of a least squares problem and application of appropriate numerical methods to find values of the design variables for minimization of the error. Pursuant to Ravani and Roth's kinematic mapping approach for mechanism synthesis, further research has been done by Bodduluri and McCarthy [15], Bodduluri [16], Larochelle [17,18], Ge and Larochelle [19], Husty et al. [20], and more recently by Wu et al. [21], Purwar and Gupta [22], and Hayes et al. [23,24]. Schrcker et al. [25] applied the kinematic mapping approach to detect branch defect in the planar four-bar linkage synthesis—a result that can be used in this work as well.

In this paper, we are dealing with the use of the image space of planar kinematics for approximate task-driven simultaneous type and dimensional synthesis of planar four-bar linkages. While the

[1]Corresponding author.

Contributed by the Design Engineering Division of ASME for publication in the Journal of Computing and Information Science in Engineering. Manuscript received December 17, 2012; final manuscript received December 12, 2016; published online May 16, 2017. Editor: Bahram Ravani.

constraint manifolds associated with planar four-bar linkages are algebraic, geometric (or, normal) distances have been used as default metric for least-squares fitting of these algebraic manifolds. Ravani and Roth [9] used normal distance to develop a least-squares algorithm for fitting the image curve of a four-bar motion. Their algorithm has two features: (1) fit the set of image points to two constraint manifolds simultaneously; and (2) use a tangent hyperplane approximation of constraint manifolds to obtain the normal distance. The resulting algorithm is highly nonlinear and requires many initial choices to converge to a reasonable solution. Larochelle [26,27] presented a different approach to the constraint manifold fitting problem that has the following two features: (1) fit the set of image points to a single constraint manifold; and (2) use a direct search method to obtain the normal distance directly. The restriction to a single manifold greatly reduces the difficulty in the fitting problem and only one random initialization is required to converge to a good solution for a *RR* dyad. Without using kinematic mapping, Yao and Angeles [28] used least-square algebraic fitting approach for dyad synthesis of planar linkages for approximate rigid body guidance. Their method is limited to *RR* type dyads only and involves solving bivariate cubic equations. More recently, Wu et al. [21] and Purwar and Gupta [22] have demonstrated a visual, computer graphics approach for multidegrees-of-freedom mechanism design that exploits the constraint manifold geometry and its apparent effect on the parameters of a mechanism to interactively perform kinematic synthesis. Hayes et al. [23,24] have presented preliminary results for combining type and dimensional synthesis of planar mechanisms for multipose rigid body guidance.

In contrast to the existing approach of trying to use the intersection curve of two algebraic manifolds for curve fitting, this paper shows that the problem of kinematic synthesis of planar four bar linkage can be solved by directly fitting a pencil of quadrics to a set of image points defining the *image curve* of a desired motion. In doing so, we use algebraic distances for least-squares fitting of quadric equations defining the constraint manifolds. This leads to a very simple and fast algorithm for linkage synthesis. The problem of fitting algebraic manifolds (or surfaces) has received considerable attention in computer aided design (CAD) and pattern recognition. A brief review of the work in this area has been presented in Ref. [7]. All the existing work for quadric surface fitting in CAD, however, deals with surface data that lead to a unique best fit surface. In kinematics, however, a given motion is mapped to a curve in the image space. Thus, the problem of quadric surface fitting in the context of kinematic mapping is fundamentally different from CAD. Since only curve data are given, the result is not a unique quadric but a pencil of quadrics that share the same curve of intersection. In this paper, we study algebraic fitting of quadric surface from this perspective and develop a new and unified method for kinematic synthesis of four-bar linkages (including both revolute and sliding joints) based on linear least-squares fitting of a pencil of quadrics.

The organization of the paper is as follows: Section 2 reviews the concept of kinematic mapping and image space in so far as necessary for the development of this paper. Section 3 presents line and circle geometric constraints associated with planar dyad motions. Section 4 deals with constraint manifolds associated with planar dyads defined by a combination of revolute and prismatic joints and presents a unified representation of a generalized manifold in the form of a general quadric. Section 5 deals with the problem of algebraic fitting of a pencil of quadric surfaces to a set of image points for an image curve defining a desired motion. In Sec. 6, we present two examples of four-bar- and one six-bar-linkages.

2 Parameterizing a Planar Displacement

A planar displacement can be decomposed into the translation of a point (d_1, d_2) on the moving body as well as rotation of the body by an angle ϕ. Let M denote a coordinate frame attached to the moving body and F be a fixed reference frame. Then, a planar displacement can be represented as a transformation of point or line coordinates from M to F. The point coordinate homogeneous transformation matrix associated with a planar displacement is given by

$$[H] = \begin{bmatrix} \cos\phi & -\sin\phi & d_1 \\ \sin\phi & \cos\phi & d_2 \\ 0 & 0 & 1 \end{bmatrix} \tag{1}$$

The line coordinate transformation for the same displacement is given by the transpose of the inverse of $[H]$ (see Ref. [13])

$$\begin{aligned}[\bar{H}] &= \left([H]^{-1}\right)^{\mathrm{T}} \\ &= \begin{bmatrix} \cos\phi & -\sin\phi & 0 \\ \sin\phi & \cos\phi & 0 \\ -d_1\cos\phi - d_2\sin\phi & d_1\sin\phi - d_2\cos\phi & 1 \end{bmatrix}\end{aligned} \tag{2}$$

The transformations $[\bar{H}]$ and $[H]$ are said to be *dual* to each other.

Introducing the following mapping from Cartesian space parameters (d_1, d_2, ϕ) to image space coordinates $\mathbf{Z} = (Z_1, Z_2, Z_3, Z_4)$ (see Ref. [9])

$$\begin{gathered} Z_1 = \frac{1}{2}\left(d_1\cos\frac{\phi}{2} + d_2\sin\frac{\phi}{2}\right),\ Z_2 = \frac{1}{2}\left(-d_1\sin\frac{\phi}{2} + d_2\cos\frac{\phi}{2}\right) \\ Z_3 = \sin\frac{\phi}{2},\ Z_4 = \cos\frac{\phi}{2} \end{gathered} \tag{3}$$

we can reparameterize the homogeneous transforms $[H]$ and $[\bar{H}]$ in quadratic form

$$[H] = \begin{bmatrix} Z_4^2 - Z_3^2 & -2Z_3Z_4 & 2(Z_1Z_3 + Z_2Z_4) \\ 2Z_3Z_4 & Z_4^2 - Z_3^2 & 2(Z_2Z_3 - Z_1Z_4) \\ 0 & 0 & Z_3^2 + Z_4^2 \end{bmatrix} \tag{4}$$

$$[\bar{H}] = \begin{bmatrix} Z_4^2 - Z_3^2 & -2Z_3Z_4 & 0 \\ 2Z_3Z_4 & Z_4^2 - Z_3^2 & 0 \\ 2(Z_1Z_3 - Z_2Z_4) & 2(Z_2Z_3 + Z_1Z_4) & Z_3^2 + Z_4^2 \end{bmatrix} \tag{5}$$

where $Z_3^2 + Z_4^2 = 1$.

Equation (3) defines a mapping from the Cartesian space parameters (d_1, d_2, ϕ) to a three-dimensional (3D) projective quasi-elliptic space parameterized by the homogeneous coordinates of the point $\mathbf{Z}$. This is called the kinematic mapping of planar displacements and the corresponding 3D projective space is called the *Image Space* of planar displacement, denoted as Σ. There is no real planar displacement that maps to the points on the real line given by $Z_3 = Z_4 = 0$. Thus, a planar displacement is represented by a point in Σ; a single degree-of-freedom (DOF) motion is represented by a curve; and a two DOF motion is represented by a surface in Σ. For details on kinematic mapping and the properties of the image space, see Refs. [9] and [13].

3 Constraining a Planar Displacement

In this paper, we consider only one- and two-DOF motions that are constrained by simple geometric constraints such as lines and circles. This includes 2DOF planar motions of a rigid body subject to one of the following four types of geometric constraints:

(1) one of its points stays on a circle: this can be realized by a planar *RR* dyad, where *R* denotes a revolute joint; see Fig. 1(*a*)

(2) one of its points stays on a line: this can be realized by a planar *PR* dyad, where *P* denotes a prismatic joint; see Fig. 1(*b*)
(3) one of its lines stays tangent to a given circle: this can be realized by a planar *RP* dyad; see Fig. 1(*c*)
(4) one of its lines translates along another line: this can be realized by a planar *PP* dyad; see Fig. 1(*d*)

A planar motion subject to any two constraints listed above (including two of the same types) results in a 1DOF motion called planar four-bar motion. Planar four-bar linkages include planar 4*R*, slider–crank, inversions of slider–crank, as well as double-slider mechanisms; see Fig. 2 for some such linkages. In this section, we develop representations of circular and linear constraints that lead to a unified representation of planar dyad motions listed above.

Let $\mathbf{X} = (X_1, X_2, X_3)$ (where $X_3 \neq 0$) denote the homogeneous coordinates of a point. Then the following equation:

$$2a_1X_1 + 2a_2X_2 + a_3X_3 = a_0\left(\frac{X_1^2 + X_2^2}{X_3}\right) \tag{6}$$

defines a circle C when $a_0 \neq 0$. The center of the circle is given by the homogeneous coordinates

$$\mathbf{a} = (a_1, a_2, a_0) \tag{7}$$

and the radius r of the circle satisfies

$$a_0^2r^2 - a_0a_3 = a_1^2 + a_2^2 \tag{8}$$

When $a_0 = 0$, Eq. (6) reduces to the equation of a line

$$2a_1X_1 + 2a_2X_2 + a_3X_3 = 0 \tag{9}$$

Thus, Eq. (6) is a unified presentation for both a circle and a line in the homogeneous form.

As a planar *RR* dyad and a *PR* dyad define, respectively, a 2DOF motion of a rigid body for which one of its points stays on a circle and on a line, Eq. (6) also provides a unified representation of geometric constraints associated with such two dyads.

We now consider an *RP* dyad that defines a 2DOF planar motion for which one of its lines stays tangent to a given circle C. This requires a line representation of a circle. First, we recast Eq. (6) in matrix form

$$[X_1\ X_2\ X_3]\begin{bmatrix} -a_0 & 0 & a_1 \\ 0 & -a_0 & a_2 \\ a_1 & a_2 & a_3 \end{bmatrix}\begin{bmatrix} X_1 \\ X_2 \\ X_3 \end{bmatrix} = 0 \tag{10}$$

The adjoint of the coefficient matrix in above is given by

$$[C_{\text{adj}}] = \begin{bmatrix} -a_0a_3 - a_2^2 & a_1a_2 & a_0a_1 \\ a_1a_2 & -a_0a_3 - a_1^2 & a_0a_2 \\ a_0a_1 & a_0a_2 & a_0^2 \end{bmatrix} \tag{11}$$

It is well known in projective geometry of conics (see Ref. [29]) that a line with coordinates $\mathbf{L} = (L_1, L_2, L_3)$ stays tangent to the circle C with center and radius given by Eqs. (7) and (8), respectively, when

$$\mathbf{L}^{\mathrm{T}}[C_{\text{adj}}]\mathbf{L} = 0 \tag{12}$$

Using Eq. (8), we can decompose $[C_{\text{adj}}]$ as

$$[C_{\text{adj}}] = \begin{bmatrix} a_1^2 & a_1a_2 & a_0a_1 \\ a_1a_2 & a_2^2 & a_0a_2 \\ a_0a_1 & a_0a_2 & a_0^2 \end{bmatrix} - \begin{bmatrix} a_0^2r^2 & 0 & 0 \\ 0 & a_0^2r^2 & 0 \\ 0 & 0 & 0 \end{bmatrix} \tag{13}$$

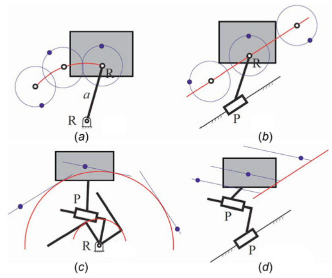

Fig. 1 Geometric constraints of a planar dyad of types: (*a*) *RR*, (*b*) *PR*, (*c*) *RP*, and (*d*) *PP*

Substituting $[C_{\text{adj}}]$ from Eq. (13) into Eq. (12), we obtain, after some algebra

$$a_1L_1 + a_2L_2 + a_0L_3 = \pm a_0r\sqrt{L_1^2 + L_2^2} \tag{14}$$

This yields two lines that are r-distance away from the center of the circle, $\mathbf{a} = (a_1, a_2, a_0)$. In addition, when $r = 0$, the two lines overlap into one that passes through $\mathbf{a}$. This is usually the case with a swinging-block type dyad.

PP dyad is a special type of dyad, whose second link actually follows a rectilinear motion with no change in orientation. The motion of a *PP* dyad is constrained such that the angle between a line $\mathbf{L} = (L_1, L_2, L_3)$ and another line $(2a_1, 2a_2, a3)$ in F is a constant, which can be described as

$$2a_1L_1 + 2a_2L_2 = k \tag{15}$$

where k is a constant that corresponds to the angle between the two lines. Equation (15) can be seen as a special case of Eq. (14). Thus, all the four planar dyads, *RR*, *PR*, *RP*, and *PP*, can be represented in terms of geometric constraints given by Eqs. (6) and (14). Furthermore, the left-hand side of Eqs. (6) and (14) is a linear combination of point and line coordinates, respectively.

4 A Unifying Representation for Planar Dyad Motions

In this section, we first derive algebraic form of a generalized quadric manifold that is common to 2DOF motions subject to the constraints containing linear and quadratic terms in Eqs. (6) and (14). We then show how this manifold can be used to develop a unified representation for constraint manifolds of planar *RR*, *PR*, *RP*, and *PP* dyads.

4.1 G-Manifolds for Planar Dyad Motions. Let $\mathbf{x} = (x_1, x_2, x_3)$ and $\mathbf{X} = (X_1, X_2, X_3)$ denote the homogeneous coordinates of a point in the moving frame M and the fixed frame F, respectively; and let $\mathbf{l} = (l_1, l_2, l_3)$ and $\mathbf{L} = (L_1, L_2, L_3)$ denote the homogeneous coordinates of a line in M and F, respectively, where $l_1^2 + l_2^2 = 1$ and the absolute value of l_3 is the distance to the line from the origin of M. An algebraic form of the constraints of the dyads parameterized by image space coordinates can be obtained by substituting the fixed frame coordinates obtained from $\mathbf{X} = [H]\mathbf{x}$ or $\mathbf{L} = [\bar{H}]\mathbf{l}$ in Eq. (6) or (14).

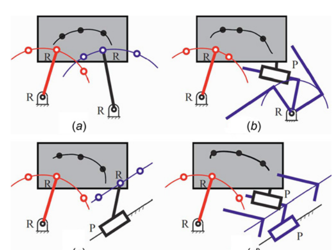

Fig. 2 Geometric constraints of some planar four-bar linkages: (*a*) *RRRR*, (*b*) *RRPR*, (*c*) *RRRP*, and (*d*) *RRPP*

In view of $\mathbf{X} = [H]\mathbf{x}$, where $[H]$ is given by Eq. (4), a linear combination of the point coordinates as shown in point constraint Eq. (6) involves only five distinct elements of the matrix $[H]$; likewise, in view of $\mathbf{L} = [\bar{H}]\mathbf{l}$, where $[\bar{H}]$ is given by Eq. (5), a linear combination of the line coordinates as shown in Eq. (14) involves only five distinct elements of the matrix $[\bar{H}]$. Furthermore, it can be shown that the nonlinear term $(X_1^2 + X_2^2)/X_3$ in Eq. (6) produces only one new element $(Z_1^2 + Z_2^2)$, and that the nonlinear term in Eq. (14) is given by

$$\sqrt{L_1^2 + L_2^2} = (Z_3^2 + Z_4^2)\sqrt{l_1^2 + l_2^2} = Z_3^2 + Z_4^2 \tag{16}$$

Thus, by collecting all of these independent terms appearing in the constraint equations, we obtain the following common representation of geometric constraints expressed by Eqs. (6) and (14) in terms of image space coordinates Z_i $(i = 1, 2, 3, 4)$:

$$\begin{aligned} q_1(Z_1^2 + Z_2^2) &+ q_2(Z_1Z_3 - Z_2Z_4) + q_3(Z_2Z_3 + Z_1Z_4) \\ &+ q_4(Z_1Z_3 + Z_2Z_4) + q_5(Z_2Z_3 - Z_1Z_4) + q_6Z_3Z_4 \\ &+ q_7(Z_3^2 - Z_4^2) + q_8(Z_3^2 + Z_4^2) = 0 \end{aligned} \tag{17}$$

This defines a quadric surface in the image space with eight homogeneous coefficients q_i $(i = 1, 2, \ldots, 8)$. In this paper, we call this quadric a *generalized constraint manifold*, or *G-manifold* in short. For this generalized-manifold to become the constraint manifold (or *C-manifold*), of a planar *RR*, *PR*, *RP*, or *PP* dyad, one must impose additional constraints on the coefficients q_i.

4.2 C-Manifolds of *RR* and *PR* Dyads. Consider first a planar 2DOF motion of a rigid body for which a point $\mathbf{x}$ on moving body remains on a circle with center (a_1, a_2, a_0) and radius r of the fixed frame, i.e., satisfies the circular constraint of Eq. (6). Substituting $\mathbf{X} = [H]\mathbf{x}$, where $[H]$ is given in Eq. (4), into Eq. (6), we obtain, after some algebra

$$\begin{aligned} &2a_1(Z_1Z_3 + Z_2Z_4) + 2a_2(Z_2Z_3 - Z_1Z_4) \\ &+ \frac{(-2a_1x_2 + 2a_2x_1)}{x_3}Z_3Z_4 + \frac{(a_1x_1 + a_2x_2)}{x_3}(Z_4^2 - Z_3^2) \\ &+ \frac{1}{2}a_3(Z_3^2 + Z_4^2) = \frac{a_0}{x_3^2}\Big(2x_3^2(Z_1^2 + Z_2^2) - 2x_1(Z_1Z_3 - Z_2Z_4) \\ &- 2x_2(Z_2Z_3 + Z_1Z_4) + \frac{1}{2x_3}(x_1^2 + x_2^2)(Z_3^2 + Z_4^2)\Big) \end{aligned} \tag{18}$$

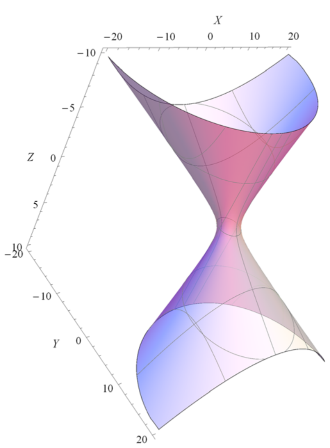

Fig. 3 A right circular hyperboloid of one sheet defined by $Z_1^2 + (Z_2 - 2Z_3)^2 - 4Z_3^2 = 5$

After collecting like terms, we obtain

$$\begin{aligned} &-2a_0x_3(Z_1^2 + Z_2^2) + 2a_0x_1(Z_1Z_3 - Z_2Z_4) + 2a_0x_2(Z_2Z_3 + Z_1Z_4) \\ &+ 2a_1x_3(Z_1Z_3 + Z_2Z_4) + 2a_2x_3(Z_2Z_3 - Z_1Z_4) + 2(a_2x_1 - a_1x_2)Z_3Z_4 \\ &-(a_1x_1 + a_2x_2)(Z_3^2 - Z_4^2) + \frac{1}{2x_3}(a_3x_3^2 - a_0x_1^2 - a_0x_2^2)(Z_3^2 + Z_4^2) = 0 \end{aligned} \tag{19}$$

We may rewrite Eq. (19) in the form of G-manifolds (Eq. (17) with the following coefficients q_i:

$$\begin{aligned} q_1 &= -2a_0x_3 \\ q_2 &= 2a_0x_1, \qquad q_3 = 2a_0x_2 \\ q_4 &= 2a_1x_3, \qquad q_5 = 2a_2x_3 \\ q_6 &= 2(a_2x_1 - a_1x_2), \qquad q_7 = -(a_1x_1 + a_2x_2) \\ q_8 &= (a_3x_3^2 - a_0x_1^2 - a_0x_2^2)/(2x_3) \end{aligned} \tag{20}$$

It follows from Eq. (20) that the coefficients q_i must satisfy the following two relations:

$$\begin{aligned} q_1q_6 + q_2q_5 - q_3q_4 &= 0 \\ 2q_1q_7 - q_2q_4 - q_3q_5 &= 0 \end{aligned} \tag{21}$$

$e = \sqrt{E}$, where

$$E = [q_1q_6 + q_2q_5 - q_3q_4]^2 + [2q_1q_7 - q_2q_4 - q_3q_5]^2 \tag{22}$$

Also e is called the *constraint fitting error*, which can be used to show if a vector $\mathbf{p}$ is qualified to represent a dyad.

Note that the coefficient q_8 is not constrained by Eq. (21) and thus can be used as the homogenizing factor. Thus, there are a total of five independent coefficients, which is consistent with the number of parameters required to define an *RR* dyad. Only a subset of the G-manifold (17) whose coefficients satisfy Eq. (21) corresponds to the C-manifolds associated with a circular constraint of Eq. (6). In particular, when $a_0 \neq 0$, we obtain the constraint manifold of a *RR* dyad whose projection onto the hyperplane $Z_4 = 1$ is a hyperboloid of one sheet [7,9,14,21]. Figure 3 shows an example of such a hyperboloid. When $a_0 = 0$, we obtain the constraint manifold of a *PR* dyad whose projection onto $Z_4 = 1$ is a hyperbolic paraboloid (Fig. 4). Furthermore, it follows from Eq. (20) that when $a_0 = 0$, one has $q_1 = q_2 = q_3 = 0$ and that both relations in Eq. (21) are automatically satisfied. This means that the constraint manifold of a *PR* dyad may be considered as a special case of that of a *RR* dyad.

4.3 C-Manifold of an *RP* Dyad. The motion of an *RP* dyad is constrained such that a line $\mathbf{l} = (l_1, l_2, l_3)$ on moving body stays tangent to a given circle C of fixed frame. Substituting $\mathbf{L} = [\bar{H}]\mathbf{l}$, where $[\bar{H}]$ is given by Eq. (5), and Eq. (16) into Eq. (14), we can put the resulting C-manifold in the same form as given by Eq. (17) where

$$\begin{aligned} q_1 &= 0, \qquad q_2 = 2a_0l_1 \qquad q_3 = 2a_0l_2 \\ q_4 &= 0, \qquad q_5 = 0, \\ q_6 &= -2a_1l_2 + 2a_2l_1, \quad q_7 = -a_1l_1 - a_2l_2, \quad q_8 = a_0(l_3 \pm r) \end{aligned} \tag{23}$$

As both l_3 and r are lumped into q_8, without any loss of generality, we may set $r = 0$, i.e., requiring that the line $\mathbf{L}$ passes through the fixed point (a_1, a_2, a_0) instead of being tangent to the circle C. The set of five nonzero coefficients $(q_2, q_3, q_6, q_7, q_8)$ are homogeneous but otherwise independent of each other. Furthermore, since $q_1 = q_4 = q_5 = 0$, it follows that Eq. (21) is automatically satisfied. Projecting this manifold onto $Z_4 = 1$, one obtains a hyperbolic paraboloid, the same type of quadric as obtained in case of a *PR* dyad.

4.4 C-Manifold of *PP* Dyad. *PP* dyad is a special type of mechanism, whose second link actually follows a translational motion with no change in orientation. The motion of a *PP* dyad is constrained such that the angle between a line $\mathbf{l} = (l_1, l_2, l_3)$ in M and a line $(2a_1, 2a_2, a3)$ in F is a constant. Substituting $\mathbf{L} = [\bar{H}]\mathbf{l}$ in Eq. (15) as in an *RP* case, we can put the resulting constraint manifold in the same form as Eq. (17) where

$$\begin{aligned} &q_1 = 0, \qquad q_2 = 0 \qquad q_3 = 0 \\ &q_4 = 0, \qquad q_5 = 0, \\ &q_6 = 2a_1 l_2 - 2a_2 l_1, \quad q_7 = a_1 l_1 + a_2 l_2, \quad q_8 = -\frac{k}{2} \end{aligned} \tag{24}$$

Since q_1 through q_5 are all equal to zero, it follows that Eq. (21) is automatically satisfied. Projecting this manifold onto $Z_4 = 1$, one obtains two parallel planes in the form of $Z_3 =$ constant. With only two equations and four unknowns to solve for, the inverse computation will result in infinite solutions. This is because the position of the line can be arbitrary for pure translation.

4.5 Inverse Computations of Dyad Parameters. A unified form of the inverse computation relationships for *RR*, *PR* or *RP* type of dyad is given as follows:

$$\begin{aligned} &l_1 : l_2 : l_3 = q_2 : q_3 : 2q_8 \\ &a_0 : a_1 : a_2 = \left(q_1^2 + q_2^2 + q_3^2\right) : \left(-q_1 q_4 - q_3 q_6 - 2q_2 q_7\right) : \\ &\left(-q_1 q_5 + q_2 q_6 - 2q_3 q_7\right) \\ &x_1 : x_2 : x_3 = \left(q_6 q_5 - 2q_7 q_4\right) : -\left(q_6 q_4 + 2q_7 q_5\right) : \left(q_5^2 + q_4^2\right) \end{aligned} \tag{25}$$

4.6 Sufficiency of the Unified Representation. From Secs. 4.1–4.5, we have found that the algebraic constraints of all the four types of planar dyads, *RR*, *PR*, *RP* and *PP*, can be converted to a unified representation given by the G-manifold (17) with two fundamental conditions (21). Conversely, it is not difficult to show that when $q_1 \neq 0$, the G-manifold (17) whose coefficients satisfy the two conditions (21) reduces to a hyperboloid of one sheet

$$\begin{aligned} &\left[q_1 Z_1 + \frac{1}{2}(q_2 + q_4)Z_3 + \frac{1}{2}(q_3 - q_5)\right]^2 \\ &+ \left[q_1 Z_2 + \frac{1}{2}(q_3 + q_5)Z_3 + \frac{1}{2}(q_2 - q_4)\right]^2 \\ &= \frac{1}{4}\left(q_2^2 + q_3^2 + q_4^2 + q_5^2 - 4q_1 q_8\right)\left(Z_3^2 + 1\right) \end{aligned} \tag{26}$$

and that when $q_1 = 0$, the G-manifold satisfying Eq. (21) reduces to a hyperbolic paraboloid

$$\begin{aligned} &Z_3[(q_3 + q_5)Z_2 + (q_7 + q_8)Z_3 + (q_2 + q_4)Z_1 + q_6] \\ &= (q_5 - q_3)Z_1 + (q_2 - q_4)Z_2 + (q_7 - q_8) \end{aligned} \tag{27}$$

Thus, it is concluded that the unified representation is both necessary and sufficient for representing all four types of planar dyads, *RR*, *PR*, *RP*, and *PP*.

4.7 Unifying Representations for Planar Four-Bar Motions. It is well known that a planar four-bar linkage can be defined by combining two planar dyads from the group of four dyads: *RR*, *PR*, *RP*, and *PP*. This results in planar 4*R*, slider–crank, inversions of slider–crank, as well as double slider mechanisms. In the past, the image curve of a planar four-bar linkage has been represented as intersection of two constraint manifolds directly associated with the two dyads. In this paper, however, we represent the image curve by a pencil of quadrics (17) that satisfy the conditions on the coefficients given by Eq. (21). Instead of fitting a pair of constraint manifolds directly, we first fit a pencil of G-manifolds (17) to the set of image points and then impose constraints (21) to identify two C-manifolds from the pencil of G-manifolds. This decoupling of constraints (21) from the curve fitting process not only removes the bottleneck in the fitting of the image curve of a four-bar linkage but also unifies the synthesis of all types of planar four-bar linkages. The choice of an *R* or *P* joint in a four-bar linkage is determined by the input positions only and is obtained *after* the fitting process for a pencil of G-manifolds.

5 Algebraic Fitting of a Pencil of G-Manifolds

Now consider the problem of fitting a pencil of G-manifolds to a set of N image points arranged such that they define an image curve rather than a surface. This problem can be formulated as an over-constrained linear problem $[A]\mathbf{q} = 0$ obtained by substituting for the given values of the image points in Eq. (17), where $\mathbf{q}$ is the column vector of homogeneous coefficients $q_i (i = 1 \ldots 8)$. The coefficient matrix $[A]$ is given by

$$[A] = \begin{bmatrix} A_{11} & A_{12} & A_{13} & A_{14} & A_{15} & A_{16} & A_{17} & A_{18} \\ \vdots & & & & & & & \vdots \\ \vdots & & & & \ddots & & & \vdots \\ \vdots & & & & & & & \vdots \\ A_{N1} & A_{N2} & A_{N3} & A_{N4} & A_{N5} & A_{N6} & A_{N7} & A_{N8} \end{bmatrix} \tag{28}$$

where for the ith image points, we have

$$\begin{aligned} &A_{i1} = Z_{i1}^2 + Z_{i2}^2, \quad A_{i2} = Z_{i1}Z_{i3} - Z_{i2}Z_{i4} \\ &A_{i3} = Z_{i2}Z_{i3} + Z_{i1}Z_{i4}, \quad A_{i4} = Z_{i1}Z_{i3} + Z_{i2}Z_{i4} \\ &A_{i5} = Z_{i2}Z_{i3} - Z_{i1}Z_{i4}, \quad A_{i6} = Z_{i3}Z_{i4} \\ &A_{i7} = Z_{i3}^2 - Z_{i4}^2, \quad A_{i8} = Z_{i3}^2 + Z_{i4}^2 \end{aligned} \tag{29}$$

5.1 Singular Value Decomposition. In linear algebra, the singular value decomposition (SVD) (see Ref. [30]) of an $N \times 8$ matrix $[A]$ is a factorization of the form

$$[A] = [U][S][V]^{\mathrm{T}} \tag{30}$$

where $[U]$ is an $N \times N$ orthonormal matrix, whose N columns, called the *left singular vectors* of $[A]$, are the eigenvectors of $[A][A]^{\mathrm{T}}$; $[S]$ is an $N \times 8$ rectangular diagonal matrix with eight non-negative real numbers on the diagonal, whose values are square roots of the eigenvalues of $[A][A]^{\mathrm{T}}$ (or equivalently

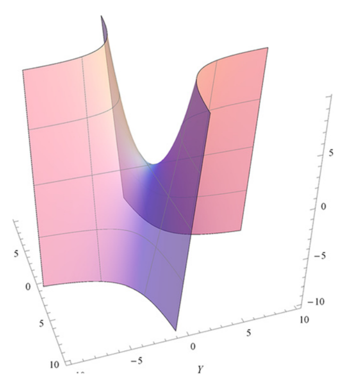

Fig. 4 A hyperbolic paraboloid defined by $Z_1 Z_2 - Z_3 = 0$

$[A]^T[A]$); and $[V]^T$ is an 8×8 orthonormal matrix, whose eight columns, called the *right singular vectors*, are the eigenvectors of $[A]^T[A]$.

The over-constrained system of linear equations, $[A]\mathbf{q}=0$, can be solved as a total least squares minimization problem with the constraint $\mathbf{q}^T\mathbf{q}=1$. The solution turns out to be the right singular vectors of $[A]$ corresponding to the least singular values. These vectors form an orthonormal set of basis vectors spanning the null space of $[A]$, or in other words, solutions to $[A]\mathbf{q}=0$. Therefore, the rank of matrix $[A]$, and consequently its nullity (8− rank), will determine the number of zero singular values.

We note that the algebraic distance fitting in SVD uses minimization of the two-norm of the error vector $[A]\mathbf{q}$ over all given image points. Such an expression is unit-inconsistent due to the fact that $[A]$ contains terms of image space coordinates, which have different dimensions (Z_1, Z_2 have dimensions of translation components, while Z_3, Z_4 are dimensionless). In order to resolve this inconsistency, it is commonly suggested that the translation vector be divided by a characteristic length L so that the translation vector is rendered dimensionless. Then, the new coordinates are given as

$$\begin{aligned}
Z_1 &= \frac{1}{2}\left(\frac{d_1}{L}\sin\frac{\phi}{2}-\frac{d_2}{L}\cos\frac{\phi}{2}\right)\\
Z_2 &= \frac{1}{2}\left(\frac{d_1}{L}\cos\frac{\phi}{2}+\frac{d_2}{L}\sin\frac{\phi}{2}\right)\\
Z_3 &= \sin\frac{\phi}{2}\\
Z_4 &= \cos\frac{\phi}{2}
\end{aligned}\tag{31}$$

When the translation components are rationalized as in above, we can use two-norm for least-square calculations. The choice of a characteristic length is discussed in detail in Ref. [31]. Another approach is to approximate a planar displacement with a spherical displacement in order to obtain a distance metric that is approximately bi-invariant and unit-consistent. This approach has been discussed in Refs. [32–36], and more recently in Ref. [37]. Purwar and Ge [37] have shown how a planar or spatial displacement can be approximated by a 3D- or four-dimensional-rotation using dual- and double-quaternion approach. Since this paper's focus is not on distance metric computation, for computational simplicity, we choose $L=1$. Any other choice of L would leave our method and algorithm unchanged. This is the choice that Ravani and Roth [9] and in recent years Hayes et al. [23,24] have also made although without explicitly mentioning it.

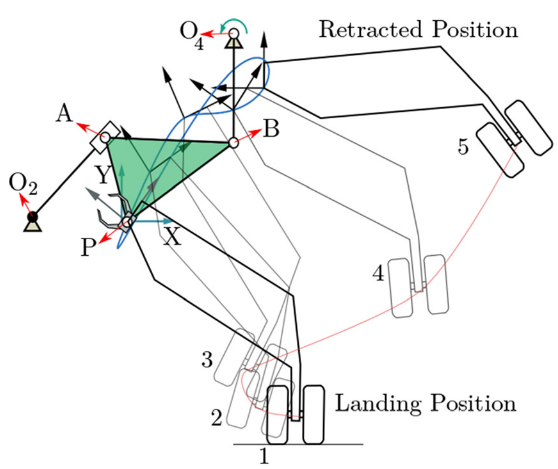

Fig. 5 Example 6.1: five positions of an aircraft landing gear labeled 1…5 are shown. The moving frame is attached to the top left corner of the housing, while frame XY is the fixed frame.

As the matrix $[A]^T[A]$ is 8×8 and positive semidefinite, all eigenvalues are non-negative and the eigenvector associated with the smallest of the eight eigenvalues is a "candidate" solution for $\mathbf{p}=(p_1,p_2,\ldots,p_8)$. When $n\le 5$, the matrix $[A]^T[A]$ has in general $(8-n)$ identical zero eigenvalues, the null space of $[A]$ is $(8-n)$ dimensional, and is defined by the corresponding orthonormal eigenvectors associated with the zero eigenvalues. Thus, a candidate solution may be expressed as a linear combination of those orthonormal eigenvectors. For $n\ge 5$, the rank of matrix $[A]$ is five, then the matrix $[A]^T[A]$ has three near-zero eigenvalues and the corresponding eigenvectors, $\mathbf{v}_\alpha$, $\mathbf{v}_\beta$, and $\mathbf{v}_\gamma$, define the basis for the null space. Let α, β, and γ denote three real homogeneous parameters. Then, any vector in the null space is given by

$$\mathbf{p}=\alpha\mathbf{v}_\alpha+\beta\mathbf{v}_\beta+\gamma\mathbf{v}_\gamma \tag{32}$$

For vector $\mathbf{p}$ to satisfy Eq. (21), we substitute Eq. (32) into Eq. (21) and obtain two homogeneous quadratic equations in (α,β,γ)

$$\begin{aligned}
K_{10}\alpha^2+K_{11}\beta^2+K_{12}\alpha\beta+K_{13}\alpha\gamma+K_{14}\beta\gamma+K_{15}\gamma^2=0\\
K_{20}\alpha^2+K_{21}\beta^2+K_{22}\alpha\beta+K_{23}\alpha\gamma+K_{24}\beta\gamma+K_{25}\gamma^2=0
\end{aligned}\tag{33}$$

where K_{ij} are defined by components of the three eigenvectors, which can be obtained from using singular value decomposition of $[A]$ [30]. As α, β, and γ are homogenous, we can set γ to be 1 in order to solve for α and β.

Solving Eq. (33) and substituting in Eq. (32) would lead to the homogeneous coordinates of dyads. For a set of n task positions, the aforementioned task analysis algorithm may yield up to four dyads from the solution of two quadratic equations in Eq. (21), two of which can be combined to form up to six four-bar linkages. Design parameters such as (x_1,x_2,x_3) and (a_0,a_1,a_2,a_3) can be obtained from inverse relationships given in Eq. (25).

In short, this approach leads to a unified algorithm for both exact synthesis (when $n\le 5$) and approximate synthesis (when $n>5$) of planar dyads that can handle joint type and dimensional synthesis simultaneously.

6 Examples

Now, we present three examples that illustrate our approach. These examples do not presume the linkage type and determine the best types and dimensions from the given motion.

6.1 Example: Motion of an Aircraft Landing Gear. Five positions for the landing gear of an aircraft are shown in Fig. 5 and listed in Table 1. The objective is to find a four-bar mechanism, which can realize this motion.

The first step of the two-step algorithm is to extract geometric constraints of motion and fit a pencil of G-manifolds to it. This is done by creating matrix [A] using Eq. (28) and applying SVD to it. Since the nullity of [A] is 3, we pick three singular vectors associated with near-zero singular values. Singular values and singular vectors are presented in Tables 2 and 3. These singular vectors form a pencil of G-manifolds defined by Eq. (32). Table 3 also contains constraint fitting error for each of the singular vectors, clearly indicating that none of them correspond to any type of mechanical dyad.

Table 1 Example 6.1: five landing gear poses

Position	x	y	Orientation (deg)
1	0.3230	−0.0400	52.5946
2	1.6205	2.6380	33.9420
3	3.6380	5.5535	24.5727
4	6.4750	5.9820	56.2930
5	8.2600	7.1725	89.7237

Table 2 Example 6.1: singular values

1509.9576	19.9563	2.1997	0.86514	0.17287	4.5937×10^{-22}	3.67426×10^{-23}	1.4156×10^{-23}

Table 3 Example 6.1: singular vectors associated with three near-zero singular values presented in Table 2

Vector	q_1	q_2	q_3	q_4	q_5	q_6	q_7	q_8	e
v_α	0.0056	0.0469	0.0165	0.2090	−0.17914	−0.9082	−0.2646	0.1640	0.0196
v_β	−0.0568	0.3128	−0.1360	0.9012	−0.07953	0.1945	0.05358	−0.1455	0.3112
v_γ	0.0273	0.0377	0.0729	−0.0745	−0.0557	0.1362	−0.8162	−0.5468	0.0384

Table 4 Example 6.1: C-manifolds obtained in the second step of fitting process, which represent two dyads of mechanism shown in Fig. 5

Vector	q_1	q_2	q_3	q_4	q_5	q_6	q_7	q_8	e
p_1	−0.01024	0.07268	−0.02362	0.06634	0.10266	0.88697	−0.11741	−0.42266	2.454×10^{-17}
p_2	-4.54×10^{-6}	1.24×10^{-5}	1.74×10^{-5}	−0.13780	0.13626	0.90545	−0.06223	−0.37245	6.446×10^{-17}

The second step is to impose constraints (33) to identify C-manifolds from the pencil of G-manifolds. Solving these equations leads to two real solutions of α, β given by

$$\begin{aligned} \alpha_1 &= -1.9303, \quad \beta_1 = 0.2417 \\ \alpha_2 &= 1.4469, \quad \beta_2 = 0.6985 \end{aligned} \tag{34}$$

Each real solution forms a C-manifold; see Table 4. It can be seen in this table that fitting error is of the order of 10^{-17}; hence, these manifolds are constraint manifolds of planar dyads. By examining the coefficients of vectors $\mathbf{p}_1$ and $\mathbf{p}_2$, it can be easily shown that first vector corresponds to the constraint manifold of an *RR* dyad ($q_1 \neq 0$), whereas the second vector corresponds to the constraint manifold of a *PR* dyad ($q_1 = q_2 = q_3 = 0$). Hence, a slider crank mechanism is formed by joining these two dyads via coupler as shown in Fig. 5. The C-manifolds projected on hyperplane $Z_4 = 1$ are shown in Fig. 6. The linkage parameters can be obtained from inverse kinematic equations (25). Parameters for dyad 1 are: $a_0 : a_1 : a_2 : a_3 = 5.9352 \times 10^{-3} : 0.0387 : 0.05989 : -109.8479$, $x_1 : x_2 : x_3 = 7.1373 : -2.3250 : 1$, while for dyad 2, they are: $a_0 : a_1 : a_2 : a_3 = 4.7822 \times 10^{-10} : 1.4528 \times 10^{-5} : 1.4365 \times 10^{-5} : -328{,}400.709$, $x_1 : x_2 : x_3 = 2.8282 : 3.7737 : 1$.

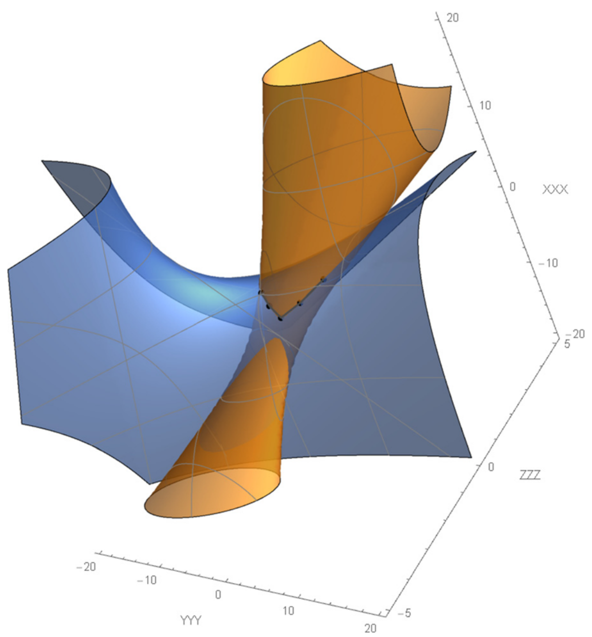

Fig. 6 Example 6.1: two resulting constraint manifolds identified from a pencil of G-manifolds that satisfy Eq. (21) are illustrated in this figure by projecting them on hyperplane $Z_4 = 1$. Intersection of hyperboloid and hyperbolic paraboloid forms constraint manifold of the slider crank mechanism. Five black image points on the intersection curve show projection of five task positions on hyperplane $Z_4 = 1$.

6.2 Example: ASME Mechanism Design Challenge. McCarthy at the 2002 ASME IDETC [38] proposed a mechanism design challenge where the objective was to synthesize a four-bar linkage to follow a motion defined by 11 poses as shown in Fig. 7. In general, such a motion can be only approximated by a four-bar linkage.

Applying our algorithm, we obtain the singular values and singular vectors as listed in Tables 5 and 6, respectively. The singular vectors form the basis for a pencil of G-manifolds. Then, we impose constraints (33) to identify C-manifolds from the pencil of G-manifolds. Solving equations (33) leads to two real solutions of α and β given by

$$\begin{aligned} \alpha_1 &= 1.4526, \quad \beta_1 = -0.5846 \\ \alpha_2 &= 1.2283, \quad \beta_2 = 1.2944 \end{aligned} \tag{35}$$

Each real solution forms a C-manifold. Table 7 contains vector coefficients corresponding to C-manifolds obtained. The projection of these C-manifolds on hyperplane $Z_4 = 1$ is depicted in Fig. 8. It can be seen in Table 7 that fitting error is of the order of 10^{-11}; hence, these manifolds are constraint manifolds of planar

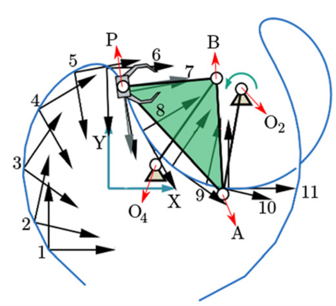

Fig. 7 Example 6.2: 11 task positions of ASME Mechanism Design Challenge and its solution as synthesized four-bar mechanism

Table 5 Example 6.2: singular values

23.37871	8.76083	4.36441	0.79490	0.152857	4.256×10^{-5}	5.378×10^{-10}	3.143×10^{-11}

Table 6 Example 6.2: singular vectors obtained from singular value decomposition

Vector	q_1	q_2	q_3	q_4	q_5	q_6	q_7	q_8	e
v_α	-4.173×10^{-4}	0.23761	0.2171	0.3202	−0.0304	−0.5980	−0.4235	−0.5058	0.1031
v_β	-1.725×10^{-5}	−0.3054	0.1746	−0.1395	−0.3229	−0.6810	0.4536	0.2878	0.1237
v_γ	0.5653	0.0481	−0.6360	−0.2299	−0.3669	−0.0805	0.0031	−0.2817	0.3029

Table 7 Example 6.2: C-manifolds corresponding to *RR* dyads of four-bar synthesized as shown in Fig. 7

Vector	q_1	q_2	q_3	q_4	q_5	q_6	q_7	q_8	e
p_1	0.17676	−0.34320	−0.25378	−0.39146	−0.28577	0.00718	0.58515	0.45736	3.065×10^{-12}
p_2	0.41615	−0.02425	−0.65091	−0.32670	−0.15971	0.50174	0.13443	0.02244	1.706×10^{-11}

dyads. After further evaluation as presented in Sec. 4.2, it can be easily concluded that each of the dyad corresponds to an *RR* dyad, which forms the four-bar mechanism depicted in Fig. 7. It is seen that the four-bar obtained in this case goes through each of the 11 poses exactly and that is because the 11 poses given were obtained from a known four-bar linkage. Using inverse kinematic equations (25), we obtain linkage parameters. The parameters for dyad 1 are: $a_0 : a_1 : a_2 : a_3 = 0.2146 : 0.4728 : 0.3483 : -4.3961$, $x_1 : x_2 : x_3 = 1.9487 : 1.3921 : 1$, and for dyad 2 they are: $a_0 : a_1 : a_2 : a_3 = 0.5942 : 0.4726 : 0.2169 : 2.2744$, $x_1 : x_2 : x_3 = 0.0615 : 1.5700 : 1$.

6.3 Example: Sit-to-Stand (STS) Motion. Now, we present an example where a linkage that can execute a sit-to-stand (STS) motion for people suffering from neuromuscular disabilities is to be synthesized. It is desirable that the orientation of the upper body to which the coupler will be attached remains constant during the STS motion. We specify five task positions with the same orientation, i.e., 0deg but the coupler goes through five different locations as shown in Table 8.

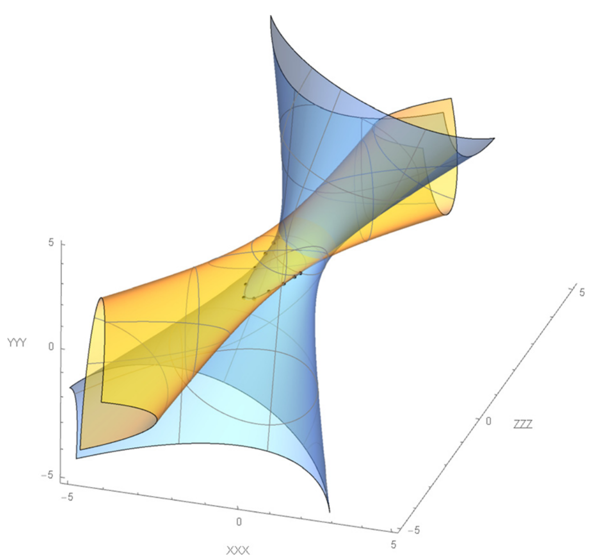

Fig. 8 Example 6.2: projection of C-manifolds tabulated in Table 7. Their intersection forms constraint manifold of the four-bar linkage. Eleven black image points on the intersection curve represent projection of task positions on hyperplane $Z_4 = 1$.

Since all five task positions share the same orientation and the positions are not on a circle, it is known that no four-bar linkage could realize this motion. So, we try to find a six bar which can realize this motion. There are many ways in which different types of six bar mechanisms can be synthesized. Here we employ Soh and McCarthy's strategy of synthesizing six-bar linkages [1], which is to start with finding a 3*R* triad to realize the task positions (Fig. 9), and then form a 1DOF closed-chain six-bar linkage by adding additional links. The process of adding a new link requires the synthesis of dyads, which are obtained by repeated application of our algorithm. For a triad shown in Fig. 9, we pick the location of fixed pivot (F1) and third joint (L1) as well as the length of the two links (links 2 and 3) between them. The given task positions are located at L1. Although there are an infinite number of triads that can reach these task positions, we pick length for links 2 and 3 to be 10.5 and 14.92, respectively, such that the triad's workspace contains the given positions; see Ref. [21] for an image-based graphical approach to selecting planar triads. Next, we use inverse kinematics to obtain the locations of joint M1 and orientations of links 2 and 3 at various task positions. Table 9 contains orientations of link 2 corresponding to each task position.

Next, we form links 4 (L1L2) and 5 (L2M3) to create a two-DOF five-bar linkage; see Fig. 10. These link lengths can be

Table 8 Example 6.3: five positions for sit to stand motion

Position	x	y	Orientation
1	−6.41	−9.80	0
2	−3.85	−10.50	0
3	−0.40	6.30	0
4	1.00	6.30	0
5	0.90	8.60	0

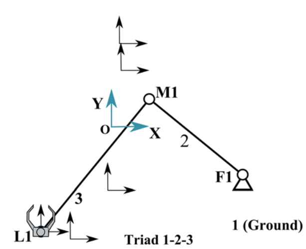

Fig. 9 Example 6.3: the synthesis starts by finding a 3*R* triad whose workspace contains the given task positions. The figure shows triad at the first task position.

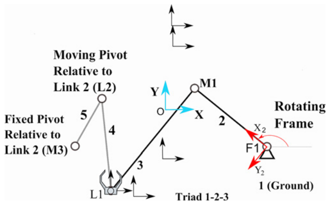

Fig. 10 Example 6.3: the figure shows a five-bar linkage, where links 4 and 5 are synthesized relative to the link 2. Figure shows locations of fixed and moving pivots of chosen dyad obtained as a result of relative synthesis.

Table 9 Example 6.3: orientations of link 2 after inverse kinematics computation

Task position	Orientation of link 2 (deg)
1	139.69
2	134.49
3	101.05
4	64.95
5	68.16

obtained by applying our algorithm to the task positions relative to link 2. We calculate location and orientation of the task positions with respect to the rotating frame X_2Y_2 located at point F1 and attached to link 2 in its corresponding orientation from Table 9. Now, we synthesize dyads that will reach these relative task positions by using our algorithm. Tables 10 and 11 present singular values and singular vectors obtained from the algorithm. Next step of the process is to impose constraints (33) to identify C-manifolds from the pencil of G-manifolds. Solving these equations leads to four real solutions of α, β given by

$$\begin{aligned} \alpha_1 &= -1.2761, & \beta_1 &= 0.4521 \\ \alpha_2 &= 0.1834, & \beta_2 &= -0.8998 \\ \alpha_3 &= -0.6259, & \beta_3 &= 0.1104 \\ \alpha_4 &= 0.1463, & \beta_4 &= 0.1105 \end{aligned} \tag{36}$$

Table 12 presents dyads obtained after second step of synthesis from which the first one, $\mathbf{p}_1$, is selected and shown in Fig. 10.

At last, as shown in Fig. 11, link 6 (F2M2) is added between links 5 and 1 and links 2 and 5 are joined to close the linkage chain and reduce the system DOF from 2 to 1. Five positions of link 5 relative to ground (link 1) are computed, and again by applying our algorithm to these positions, we obtain four feasible dyads. Tables 13–15 present singular values, singular vectors, and dyads obtained in the synthesis process, respectively. Four solutions to Eq. (33) in the second step of synthesis are given by

$$\begin{aligned} \alpha_1 &= -0.0030, & \beta_1 &= 0.0654 \\ \alpha_2 &= -0.0265, & \beta_2 &= 0.6965 \\ \alpha_3 &= -0.0092, & \beta_3 &= 0.0791 \\ \alpha_4 &= 0.0411. & \beta_4 &= 0.9517 \end{aligned} \tag{37}$$

It is obvious that one of the resulting dyad should be the existing coupler link 2. The other three feasible ground joints are:

Table 10 Example 6.3: singular values obtained in relative synthesis of links 4 and 5

22,209	92.271	15.0021	0.23189	0.01793	7.7724×10^{-12}	4.1753×10^{-13}	2.4375×10^{-13}

Table 11 Example 6.3: singular vectors associated with near-zero singular values presented in Table 10

Vector	q_1	q_2	q_3	q_4	q_5	q_6	q_7	q_8	e
v_α	−0.0399	0.0343	0.0120	0.4074	0.0847	−0.9018	−0.1025	0.0121	0.1564
v_β	−0.0464	0.1559	−0.1646	0.3061	0.0742	0.0465	0.9193	0.0123	0.0574
v_γ	−0.0229	−0.0222	0.0164	0.2623	−0.0206	0.1268	−0.08658	0.9517	0.1463

Table 12 Example 6.3: C-manifolds obtained in relative synthesis of links 4 and 5

Vector	q_1	q_2	q_3	q_4	q_5	q_6	q_7	q_8	e
p_1	7.15×10^{-3}	4.26×10^{-3}	−0.0733	−0.1191	−0.0952	1.2988	0.4599	0.9518	4.65×10^{-13}
p_2	0.0115	−0.1558	0.1668	0.0615	−0.0718	−0.0805	−0.9326	0.9517	7.69×10^{-14}
p_3	-3.14×10^{-3}	−0.0265	-9.22×10^{-3}	0.0411	−0.0654	0.6965	0.0791	0.9517	6.54×10^{-14}
p_4	−0.0334	-4.40×10^{-13}	-1.63×10^{-13}	0.3557	-4.36×10^{-13}	1.72×10^{-12}	2.31×10^{-12}	0.9517	2.35×10^{-13}

Table 13 Example 6.3: singular values obtained in synthesis of link 6

12,164	231.45	24.2207	6.0531	2.0841	7.7724×10^{-12}	4.1753×10^{-13}	2.4375×10^{-13}

Table 14 Example 6.3: singular vectors associated with zero singular values presented in Table 13

Vector	q_1	q_2	q_3	q_4	q_5	q_6	q_7	q_8	e
v_α	−0.0137	-1.14×10^{-3}	-4.63×10^{-3}	0.1287	-0.062×10^{-3}	-6.04×10^{-3}	−0.0458	0.9885	0.2416
v_β	0.0161	0.0653	0.0148	0.02145	−0.1055	0.9896	0.0650	0.0123	0.1432
v_γ	−0.0191	−0.0103	−0.0934	−0.3013	0.0750	0.0788	−0.9424	0.4363	0.1624

Table 15 Example 6.3: C-manifolds obtained in synthesis of link 6

Vector	q_1	q_2	q_3	q_4	q_5	q_6	q_7	q_8	e
p_1	0.2637	-6.90×10^{-13}	1.462×10^{-12}	-2.988	1.393	-1.291×10^{-11}	7.774×10^{-12}	-20.597	1.265×10^{-17}
p_2	0.0251	0.06591	-0.0678	-0.5214	0.0736	1.2117	-0.7815	-1.877	3.645×10^{-17}
p_3	-0.099	-0.5245	-0.1955	-0.9108	1.123	-7.746	-1.3016	-3.3733	4.565×10^{-13}
p_4	0.0159	0.1267	-0.0618	-0.2698	-0.1396	2.1539	-0.8012	-0.1034	1.464×10^{-12}

Table 16 Example 6.3: location for pivots when mechanism is at the first pose

Name of pivot	x	y
F1	11.329	-5.283
M1	3.321	1.509
L1	-6.410	-9.800
M3	-10.309	-4.651
L2	-7.196	0.601
M2	-9.308	0.908
F2	-9.190	11.341

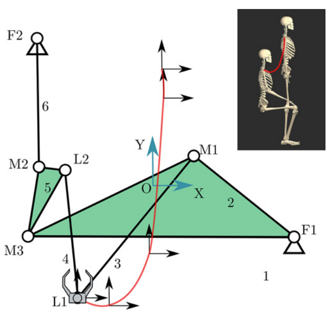

Fig. 11 Example 6.3: the synthesized six-bar linkage for the generation of sit-to-stand motion at the first task position. Image at top right corner shows curve traced by shoulder joint of the human skeleton performing sit to stand motion.

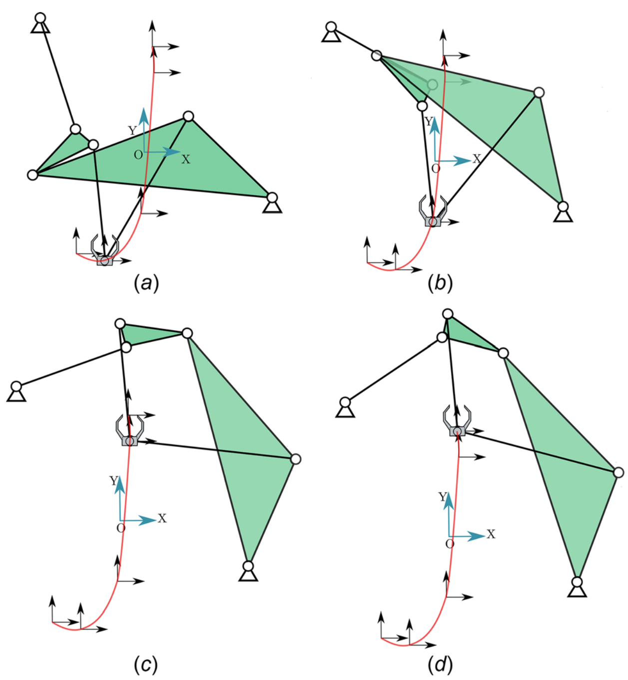

Fig. 12 Example 6.3: the sit-and-stand six-bar linkage at task positions 2, 3 (top) and 4, 5 (bottom)

(20.7068, -2.92409), (-9.19081, 11.3414), and (16.9025, 8.74652). The corresponding lengths of link 6 are 30.2593, 10.4335, and 27.358. We select link 6 (F2M2) to have the ground joint with coordinates (-9.19081, 11.3414) and link length of 10.4335. Figure 11 shows the synthesized Watt I six-bar linkage at the first position. At this position, the coordinates of seven pivots of the six bar are presented in Table 16. Figure 12 shows the synthesized Watt I six-bar linkage passing through the remaining four specified task positions. This example has demonstrated that by repeated application of the same algorithm, planar six-bar linkages with both revolute and prismatic joints can also be synthesized.

7 Conclusions

In this paper, we presented a novel method for synthesizing planar motion using kinematic mapping. Instead of finding two special quadric constraint manifolds associated with a four-bar linkage with nonlinear (quadratic) coefficients, which makes the problem difficult to solve, we used a more general form of quadric such that its coefficients are linear. Furthermore, we seek to fit a given set of image points to a pencil of quadrics. This leads to a linear least squares problem that can be readily solved using SVD algorithm. After obtaining the pencil of quadrics that contains the constraint manifolds, we then impose the quadratic constraints associated with the constraint manifold to find the two special quadrics. The resulting algorithm for planar four-bar linkage synthesis is not only vastly more efficient but also unifies the treatment of dyads composed from revolute joints and sliding joints. We also showed that by applying the same algorithm twice, planar six-bar linkages can also be synthesized.

Acknowledgment

This work has been financially supported by National Science Foundation under a research grant to Stony Brook University (A. Purwar and Q. J. Ge, Grant No. CMMI-1563413). All findings and results presented in this paper are those of the authors and do not represent those of the funding agencies.

References

[1] McCarthy, J. M., and Soh, G. S., 2010, *Geometric Design of Linkages*, 2nd ed., Springer, Berlin.
[2] Sandor, G. N., and Erdman, A. G., 1997, *Advanced Mechanism Design: Analysis and Synthesis*, Vol. 2, Prentice-Hall, Upper Saddle River, NJ.
[3] Hunt, K., 1978, *Kinematic Geometry of Mechanisms*, Oxford University Press, Oxford, UK.
[4] Hartenberg, R. S., and Denavit, J., 1964, *Kinematic Synthesis of Linkages*, McGraw-Hill, New York.
[5] Suh, C. H., and Radcliffe, C. W., 1978, *Kinematics and Mechanism Design*, Wiley, New York.
[6] Wu, J., Ge, Q. J., Su, H.-J., and Gao, F., 2010, "Kinematic Acquisition of Geometric Constraints for Task Centered Mechanism Design," ASME Paper No. DETC2010-28287.
[7] Ge, Q. J., Zhao, P., Purwar, A., and Li, X., 2012, "A Novel Approach to Algebraic Fitting of a Pencil of Quadrics for Planar 4R Motion Synthesis," ASME J. Comput. Inf. Sci. Eng., **12**(4), p. 041003.
[8] Burmester, L. E. H., 1888, *Lehrbuch der Kinematik*, A. Felix, Leipzig, Germany.
[9] Ravani, B., and Roth, B., 1983, "Motion Synthesis Using Kinematic Mappings," ASME J. Mech., Transm., Autom. Des., **105**(3), pp. 460–467.
[10] Ravani, B., and Roth, B., 1984, "Mappings of Spatial Kinematics," ASME J. Mech., Transm., Autom. Des., **106**(3), pp. 341–347.
[11] Blaschke, W., 1911, "Euklidische Kinematik und Nichteuklidische Geometrie," Z. Math. Phys., **60**, pp. 61–91; 203–204.

[12] Grunwald, J., 1911, "Ein Abbildungsprinzip, Welches die Ebene Geometrie und Kinematik mit der Raumlichen Geometrie Verknupft," Sitzungsber. Akad. Wiss. Wien, **120**, pp. 677–741.
[13] Bottema, O., and Roth, B., 1979, *Theoretical Kinematics*, North Holland, Amsterdam, The Netherlands.
[14] McCarthy, J. M., 1990, *Introduction to Theoretical Kinematics*, MIT Press, Cambridge, MA.
[15] Bodduluri, R. M. C., and McCarthy, J. M., 1992, "Finite Position Synthesis Using Image Curve of a Spherical Four-Bar Motion," ASME J. Mech. Des., **114**(1), pp. 55–60.
[16] Bodduluri, R., 1990, "Design and Planned Movement of Multi-Degree of Freedom Spatial Mechanisms," Ph.D. dissertation, University of California, Irvine, CA.
[17] Larochelle, P., 1994, "Design of Cooperating Robots and Spatial Mechanisms," Ph.D. dissertation, University of California, Irvine, CA.
[18] Larochelle, P., 1996, "Synthesis of Planar RR Dyads by Constraint Manifold Projection," Proceedings of the ASME Design Engineering Technical Conferences, Irvine, CA, Aug. 18–22.
[19] Ge, Q. J., and Larochelle, P. M., 1999, "Algebraic Motion Approximation With Nurbs Motions and Its Application to Spherical Mechanism Synthesis," ASME J. Mech. Des., **121**(4), pp. 529–532.
[20] Husty, M. L., Pfurner, M., Schrocker, H.-P., and Brunnthaler, K., 2007, "Algebraic Methods in Mechanism Analysis and Synthesis," Robotica, **25**(6), pp. 661–675.
[21] Wu, J., Purwar, A., and Ge, Q. J., 2010, "Interactive Dimensional Synthesis and Motion Design of Planar 6R Single-Loop Closed Chains Via Constraint Manifold Modification," ASME J. Mech. Rob., **2**(3), p. 31012.
[22] Purwar, A., and Gupta, A., 2011, "Visual Synthesis of RRR- and RPR-Legged Planar Parallel Manipulators Using Constraint Manifold Geometry," ASME Paper No. DETC2011-48830.
[23] Hayes, M. J. D., Luu, T., and Chang, X.-W., 2004, "Kinematic Mapping Application to Approximate Type and Dimension Synthesis of Planar Mechanisms," *9th Advances in Robotic Kinematics*, Kluwer Academic Publishers, Dordrecht, The Netherlands.
[24] Hayes, M. J. D., and Rucu, S. R., 2011, "Quadric Surface Fitting Applications to Approximate Dimensional Synthesis," 13th World Congress in Mechanism and Machine Science, Guanajuato, Mexico, June 19–25.
[25] Schrcker, H.-P., Husty, M. L., and McCarthy, J. M., 2007, "Kinematic Mapping Based Assembly Mode Evaluation of Planar Four-Bar Mechanisms," ASME J. Mech. Des., **129**(9), pp. 924–929.
[26] Larochelle, P., 2000, *Approximate Motion Synthesis Via Parametric Constraint Manifold Fitting*, Kluwer Academic Publishers, Dordrecht, The Netherlands, pp. 103–110.
[27] Larochelle, P., 2003, "Approximate Motion Synthesis of Open and Closed Chains Via Parametric Constraint Manifold Fitting: Preliminary Results," ASME Paper No. DETC2003/DAC-48814.
[28] Yao, J., and Angeles, J., 2000, "Computation of All Optimum Dyads in the Approximate Synthesis of Planar Linkages for Rigid-Body Guidance," Mech. Mach. Theory, **35**(8), pp. 1065–1078.
[29] Sommerville, D., 1959, *Analytical Geometry of Three Dimensions*, Cambridge University Press, New York.
[30] Golub, G., and Van Loan, C., 1996, *Matrix Computations*, Johns Hopkins University Press, Baltimore, MD.
[31] Angeles, J., 2006, "Is There a Characteristic Length of a Rigid-Body Displacement?," Mech. Mach. Theory, **41**(8), pp. 884–896.
[32] Etzel, K., and McCarthy, J. M., 1996, "A Metric for Spatial Displacements Using Biquaternions on so(4)," IEEE International Conference on Robotics and Automation, Minneapolis, MN, April 22–28, pp. 3185–3190.
[33] Etzel, K., and McCarthy, J. M., 1996, "Spatial Motion Interpolation in an Image Space of so(4)," ASME Paper No. 96-DETC/MECH-1164.
[34] Larochelle, P., Murray, A., and Angeles, J., 2007, "A Distance Metric for Finite Sets of Rigid-Body Displacements Via the Polar Decomposition," ASME J. Mech. Des., **129**(8), pp. 883–886.
[35] Larochelle, P., 2006, "A Polar Decomposition Based Displacement Metric for a Finite Region of SE(n)," *Advances in Robot Kinematics* (ARK), B. R. J. Lenarcic, ed., Springer, Berlin.
[36] Larochelle, P., and Murray, A., 2005, "Projection Metrics for Rigid-Body Displacements," ASME Paper No. DETC2005-84698.
[37] Purwar, A., and Ge, Q. J., 2012, "Polar Decomposition of Unit Dual Quaternions," ASME J. Mech. Rob., **5**(3), p. 031001.
[38] McCarthy, J. M., 2002, "Special Session on Computer Aided Linkage Synthesis," ASME International Design Engineering Technical Conference, Montreal, QC, Canada, Sept. 29–Oct. 2.